Scientia Iranica D (2023) 30(4), 1350–1367

SCIENTIA IRANICA

Sharif University of Technology

Scientia Iranica

Transactions D: Computer Science & Engineering and Electrical Engineering

http://scientiairanica.sharif.edu

Fast and secure angular-based detection algorithm for reverse power occurrence in synchronous generators

M. Samami[a] and M. Niaz Azari[b,*]

a. *Department of Electrical Engineering, Sari Branch, Islamic Azad University, Sari, Iran.*

b. *Department of Electrical Engineering, University of Science and Technology of Mazandaran, Behshahr, P.O. Box 48518-78195, Iran.*

Received 24 May 2021; received in revised form 6 September 2021; accepted 1 November 2021

KEYWORDS

Directional relay;
Internal voltage;
Load angle;
Prime mover;
Reverse power;
Synchronous generator.

Abstract. Reverse Power (RP) phenomenon in synchronous generators may lead to severe damage to the generator prime mover due to the motoring action of the generator. The operation of the usual technique, which detects RP on the basis of current direction, is too slow because of utilization of intentional time delay in the relay structure. The deliberate time delay helps the relay to avoid tripping during unwanted disturbances. This paper proposes a novel angular-based scheme to detect RP in synchronous generators. To this end, the proposed technique uses the load angle (δ) and the phase difference between voltage and current (θ), as the angular quantities of the generator. Furthermore, other electrical parameters of the generator such as current and voltage are utilized as the supplementary parameters for RP detection. Ultimately, this contribution uses the analysis of vertical component of E_A ($E_A \sin\delta$) and the tangential component of I_A on V ($I_A \cos\theta$) in the generator phasor diagram for making the final decision. To verify the performance of the angular-based technique, extensive simulations are carried out on two sample systems (single-machine and three-machine infinite buses) under different conditions, and the final results show the satisfactory performance of the proposed algorithm.

1. Introduction

Reverse Power Condition (RPC) occurs when the prime mover of a synchronous generator fails. Under this condition, the generator starts to work the same as a synchronous motor and the prime mover (turbine or engine) acts like an active load for the motor. This phenomenon might lead to serious damage to the prime mover due to a significant rise in steam temperature, turbine blade damage in steam and gas turbines, and blade or runner cavitation in hydraulic turbines [1].

Therefore, fast and reliable detection of RPC is essential in order to prevent severe damages to the generator prime mover. To this end, Reverse Power Relays (RPR) are widely utilized as the main protection of generators against RPC [2].

Until today, there have been limited schemes for Reverse Power Protection (RPP) [2–7]. Directional method is known as the most famous technique for RPP [3,4]. Directional relays work on the basis of power flow direction. In fact, the mentioned relays send the trip signal to the generator circuit breaker

*. *Corresponding author. Tel.: +98 11 34556000*
E-mail addresses: mehdisamami63@gmail.com (M. Samami); miladniazazari@mazust.ac.ir (M. Niaz Azari)

doi: 10.24200/sci.2021.58407.5711

when the direction of power is from the network to the generator. It is noteworthy that directional relays employ an intentional time delay in order to prevent potential mal-operation of the relay during disturbances of the power network. This issue is considered as the main drawback of these relays due to increase in the motoring time of the generator, which might lead to severe damage to the generator mover. Clark and Feltes [2] analyzed the behavior of a group of generators in the islanding mode. However, the proposed method of this study has two problems. The first one refers to oscillations of active power after Reverse Power (RP) occurrence. In this condition, the output power might return above the RP threshold and reset the timer of the RPR. Hence, in order to prevent mal-operation, the relay should not operate before reducing power oscillations. Furthermore, the need to perform precise adjustment of the governor droop in order to compensate the initial loading of the generator is considered as the second problem of the mentioned method. Jenkins et al. [5] applied two novel logics for detection of RPC. The first one is time dependent, while the second one is double threshold. The presented methods improve the performance of the conventional RPR, considering the influence of initial overshoot caused by steam turbine valve closure and the frequency of its oscillations. The delay element used in the structure of this relay postpones its performance and is known as the main drawback of this study. Another contribution [6] discussed finding a proper direction in the directional active power, reactive power, and current RPR on the basis of power network phase rotation. The mentioned relays cannot remove the generator from the grid as quickly as expected. Thus, the potential damage to the prime mover is considered as the main concern in these relays. Yaghobi [7] introduced a new flux-based RPR on the basis of two key parameters including angular velocity and acceleration. These parameters are estimated from the generator air-gap flux. The action results of the flux-based RPR show the faster performance of this relay than conventional relay. However, measuring and estimation of the air-gap flux is too hard and costly, which needs extra equipment. As a result, this issue is considered as the main drawback of this method. Samami and Niaz Azari [8] detected RPC using some electrical parameters on the basis of differences between over and under excitation modes in lagging and leading operations of synchronous motors and generators. The mentioned method improved the operation time of the relay in comparison with directional and flux-based methods. However, the speed of operation and also, the reliability and fault discrimination of this method can still be reinforced. It is noteworthy that over the past years, all the investigations into RPP were limited in [2–8]. However, in recent years, various contributions have been presented for generator protection against possible faults such as Loss Of Excitation (LOE) and Out Of Step (OOS). The mentioned studies use various parameters of the generator such as active power (P) [9], impedance (Z) [10,11], air-gap flux (φ), and a combined benchmark of other parameters including load angle (δ), stator terminal voltage (V) or current (I_A), and reactive power for LOE detection [12–18]. Besides, OOS is considered another important protection that can be detected by P and δ on the basis of equal area criteria [19–24]. Thus, suitable operation of the aforementioned techniques in detecting various potential faults and, also, better performance of parameter-based RPR [8] in comparison with conventional directional methods in synchronous generators have become the most significant motivations for the authors to present a new technique for generator RPP in order to enhance the accuracy and speed of the previously introduced schemes.

This investigation presents a novel angular-based predictive technique to detect RPC in synchronous generators. The approach applies the analysis of some electrical parameters of the generator including δ and the phase difference between voltage and current (θ) as the angular quantities and V, I_A, internal voltage (E_A), and P as the supplementary quantities in the detection algorithm. Finally, the RPC is detected based on two criteria, namely the sign of vertical component of E_A ($E_A \sin\delta$) and the tangential component of I_A on V ($I_A \cos\theta$). As a matter of fact, this study presents an improved algorithm with almost identical parameters, higher operation speed, and better fault diagnosis than the parameter-based method [8], which was previously published by the authors. To demonstrate the satisfactory performance of the suggested scheme, the operation of the angular-based RPR is evaluated in two power systems with various prime movers and loads and is compared with directional, flux-based, and parameter-based techniques. According to the results, it can be concluded that the proposed RPR exhibits the best performance, considering different prime movers, droop setting of governor, and loadings. Besides, the mentioned results indicate that the proposed method has the highest speed, accuracy, and reliability to detect RPC among other methods.

The rest of this investigation is organized as follows. Section 2 describes the construction and operation of the conventional (directional) RPR. The behavior of the generator electrical parameters under RPC is presented in Section 3. The proposed technique is completely introduced and analyzed in Section 4. In Section 5, extensive simulations are carried out to confirm the angular-based relay performance in different scenarios. Section 6 presents the comparative analysis as the final validation. Finally, this study is concluded in Section 7.

2. The construction and principle of operation of conventional RPP

The directional-based scheme is the usual and most popular technique to detect the reverse power phenomenon. According to Figure 1, the directional RP relay is constructed from a light non-magnetic aluminum disc between two soft laminated iron cores and is fixed on a spindle, running on low friction bearings. The upper iron core is wound with a voltage winding which is then supplied from one phase and an artificial neutral of the generator output. Another core has a current winding which is supplied by a current transformer connected to the same phase as the voltage in the other core. Since the voltage winding has a huge amount of inductance, the current leads the voltage by an approximate value of 90°. Accordingly, the magnetic field generated by the current winding leads the magnetic field generated by the voltage winding. The mentioned fields supply a motivation current in the relay disc. This current produces a mechanical torque, which leads to the rotation of the disc. In RPC, the disc rotates in the opposite direction and moves away from the stop and towards the trip contacts, leading to the activation of the trip circuit.

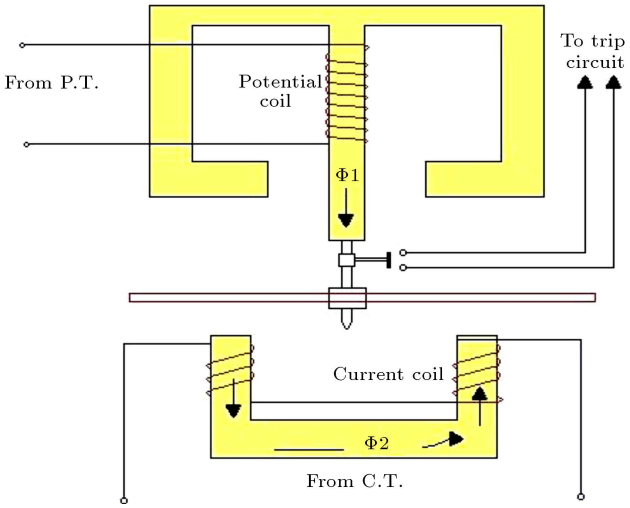

Figure 1. Construction of the conventional RPR.

In other words, the occurrence of RPC leads to the formation of a specified phase shift with the value of 180° in the stator current. The mentioned angle is known as the Maximum Torque Angle (MTA). The vector diagram of voltage and current following RPC considering the directional relay system is obviously depicted in Figure 2. Accordingly, the normal and RP flow of a synchronous machine can be diagnosed in accordance to the value of θ ($-90 < \theta < 90$ for normal condition and $90 < \theta < 270$ for RPC) [25].

As a result, the use of directional relays with the MTA value of 180° is helpful in detecting the reverse current flow. In order to prevent the mal-operation of RPR during synchronization and potential disturbances, a delay time is utilized in RPR. This time delay postpones the relay trip time for almost 5 to 7 s following RPC. This issue is considered the main drawback of the conventional electro-mechanical or digital RPR, because the utilization of intentional time delay enhances the generator motoring time and the mechanical stress to the prime mover. It is noteworthy that the theory behind the performance of digital protection (numerical) relays is extremely the same as old conventional directional relays. On the other hand, digital relays still suffer from the deliberate delay time in order to avoid potential mal-operation. Thus, presenting a novel fast and reliable RPD method seems to be essential to overcome this problem.

3. Variations of electrical quantities during RPC

As stated earlier, in RPC, the synchronous machine operation mode changes from generating to motoring condition. This issue has significant effect on the behavior of the generator electrical quantities such as voltages and angular values [26]. As demonstrated in [27], per phase V_ϕ and E_A are interdependent in accordance to the following equations for generators and motors, respectively.

$$V_{\phi(gen)} = E_A - R_A I_A - jX_S I_A, \tag{1}$$

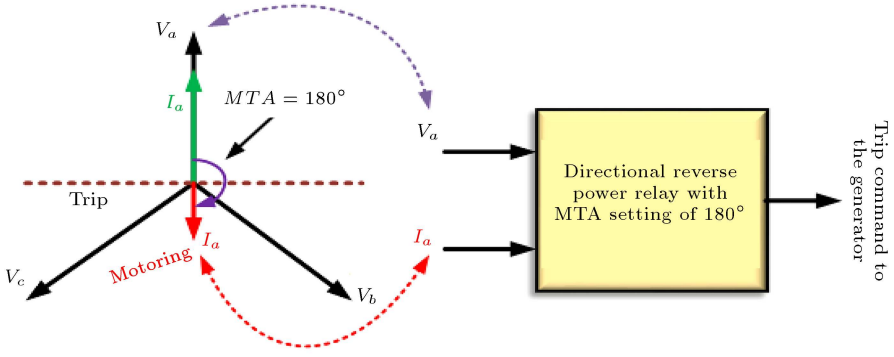

Figure 2. Phasor diagram of current and voltage under RPC, considering the directional RPR system.

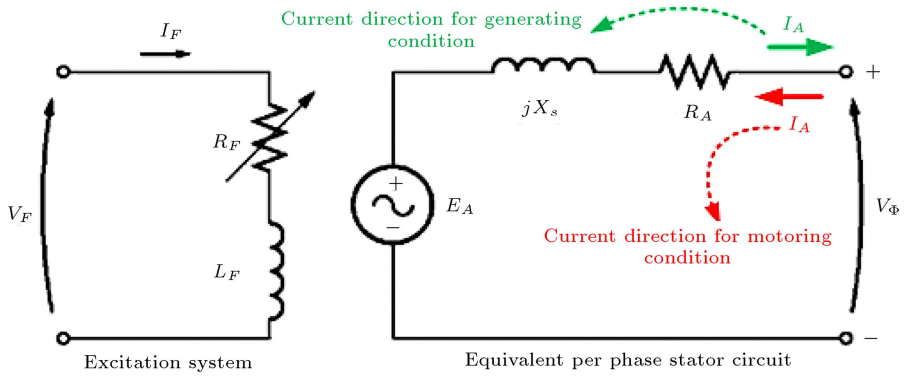

Figure 3. Per phase equivalent circuit of a synchronous machine.

$$V_{\phi(mot)} = E_A + jX_S I_A + R_A I_A, \tag{2}$$

where $R_A I_A$ is the voltage drop arising from the stator winding resistance and $jX_S I_A$ represents the effect of both armature reaction and the voltage drop originating from the self-inductance of the stator winding. It is worth highlighting that the distinction of V_ϕ for generators and motors stems from the opposite flow of stator current in the equivalent circuit of motors compared with generators. The equal per phase circuit for synchronous machines is illustrated in Figure 3.

Furthermore, the load or torque angle (δ) is considered as one of the most decisive angular parameters of synchronous machines obtained by subtracting the terminal voltage angle from internal voltage angle ($\angle E_A - \angle V_\phi$) [27].

From another perspective, the load angle is the angle between rotor magnetic field (B_r) and stator magnetic field (B_s). The condition of synchronism is the simultaneous rotation of these two fields at a synchronous speed.

In the generating mode, B_r leads B_s , while in the motoring mode, B_r follows B_s (see, Figure 4) [7]. Accordingly, in the generating condition, δ is positive, while it is negative in the motoring condition. As a result, δ is expected to be negative following RPC.

Another important angular parameter is the angle between the voltage and current (θ). The positive and negative values of θ indicate the lagging and leading operation of the machine, respectively. Figure 4 shows the phasor diagram of a synchronous machine in both motoring and generating modes of operation, considering the variations of all the explained parameters.

4. The proposed method

4.1. Developing the idea

This contribution uses the angular quantities (δ and θ) as the main parameters for RPD. Furthermore, V_ϕ, E_A, I_A, and P are considered as the complimentary criteria for this aim. Therefore, the variations of the aforementioned parameters should be analyzed for both normal condition and RPC.

In order to calculate the internal voltage of the generator (E_A), two methods are employed. The first one is on the basis of generator equations mentioned in Eqs. (1) and (2). Since all the parameters of the aforementioned equations, except E_A, are specified by measurement or specification of the generator, the internal voltage can be calculated easily.

Furthermore, the internal voltage can be calculated by the following equation [27]:

$$E_A = \sqrt{2}\pi N_C \phi f, \tag{3}$$

where N_C represents the generator construction, ϕ the flux, and f the frequency of the generator. As a result, E_A is directly dependent on the flux and speed of the machine. It is noted that the flux variation is affected by changes in the generator field current (I_f) and the field current is also affected by the network behavior. The air-gap flux can be measured based on Faraday's law of induction by means of search coil sensors, located along the stator teeth [7,15].

Among the mentioned parameters, δ is too hard to measure. Therefore, $\Delta\delta$ can be estimated using a typical technique on the basis of swing equation for the specified generator as follows [13,28]:

$$\frac{d^2\delta(t)}{dt^2} = \frac{\pi f_0}{H}(P_M - P_E), \tag{4}$$

where f_0, H, P_M, and P_E represent fundamental frequency, inertia constant, mechanical input power, and electrical output power, respectively. Of note, P_M is a constant value that is equal to P_E in a steady state condition.

By integrating both sides of Eq. (4) over Δt, Eq. (5) is obtained:

$$\frac{d\delta(t)}{dt}\Big]^{t} - \frac{d\delta(t)}{dt}\Big]^{t-\Delta t} = \frac{\pi f_0}{H}\int_{t-\Delta t}^{t}(P_M - P_E)\,dt. \tag{5}$$

The right-side expression of Eq. (5) can be estimated by the trapezoidal relation as follows:

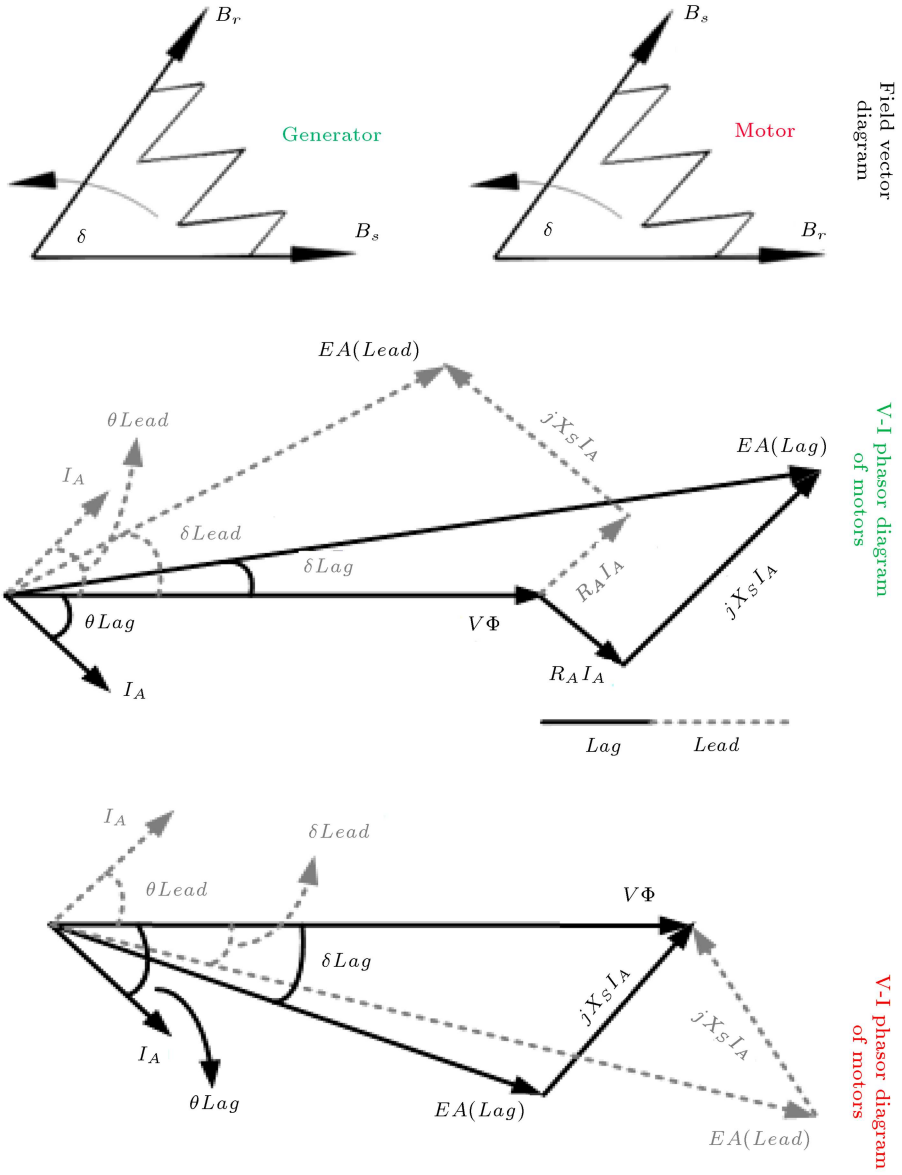

Figure 4. The V-I phasor diagram and the field vector diagram of a synchronous machine.

$$\frac{\pi f_0}{H}\int_{t-\Delta t}^{t}(P_M - P_E)\,dt$$

$$= \frac{\pi f_0}{H}\frac{(2P_M - P_E)^t - P^{t-\Delta t}}{2}\Delta t. \quad (6)$$

By inserting Eq. (6) into Eq. (5), the final relation is given below:

$$\frac{\Delta\delta^t}{\Delta t} = \frac{\Delta\delta^{t-\Delta t}}{\Delta t} + \frac{\pi f_0}{H}\frac{(2P_M - P_E)^t - P^{t-\Delta t}}{2}\Delta t. \quad (7)$$

Consequently, the load angle variation at each instant can be written as follows:

$$\Delta\delta^t = \Delta\delta^{t-\Delta t} + \frac{\pi f_0}{H}\frac{(2P_M - P_E)^t - P^{t-\Delta t}}{2}\Delta t^2. \quad (8)$$

However, $\Delta\delta$ can be approximated by another technique, as expressed in Eq. (9), in which ω and ω_0 are the measured and synchronous speeds of the generator, respectively [13]. However, this study applied Eq. (8) for $\Delta\delta$ estimation.

$$\Delta\delta^t = \left(\omega^t - \omega_0\right)\Delta t. \quad (9)$$

As stated earlier, P was introduced as another decisive quantity for RPD. Accordingly, the 3-phase active power (P_{3ph}) can be written as follows [8,29]:

$$P_{3ph}(t) = P_4 + P_5 t^2.e^{-(2t/\tau)} + P_6 t.e^{-(t/\tau)}.$$
$$\sin\left(2\pi f_{slip}t + \alpha\right) + P_7 t^2.e^{-(2t/\tau)}.$$
$$\cos\left(4\pi f_{slip}t + 2\alpha\right), \quad (10)$$

Table 1. The behavior of δ and P_{3ph} in different operating conditions of a synchronous machine.

Generating mode	Initial moments of prime mover failure	Motoring mode
$\delta > 0$	$\Delta\delta/\Delta t \neq 0$	$\delta < 0$
$P_{3ph} > 0$	$\Delta P_{3ph}/\Delta \neq 0$	$P_{3ph} < 0$

where P_4, P_5, P_6, P_7, and α are constant values. τ is the damping time constant of the speed and f_{slip} represents the slip frequency that is related to rotor speed variations. It is worth highlighting that due to the greater value of f_{slip} than $2f_{slip}$, the active power oscillates with only one frequency (f_{slip}), following the RPF [8,29]. The range of f_{slip} variations is from 0.3 to 7 Hz [29]. Figure 5(a) shows the variations of both δ and P_{3ph} of a synchronous machine in a RPC. Accordingly, the mentioned values have the same behavior in different modes of operation of a synchronous machine. The oscillations of δ at initial moments of the prime mover outage and finally, damping of the mentioned oscillations in the motoring mode indicate that the synchronous generator retains its stability following the RPF (reverse power fault). This is because in an unstable condition which may occur during an external fault or LOE condition, δ exhibits an absolute increasing behavior (see, Figures 5(b) and (c)) [12,13]. Of note, the behavior of δ and P_{3ph} is summarized in Table 1.

This study uses three criteria as the initial prerequisites of RPD. The first one is based on the ratio of $|E_A|$ to $|V_\phi|$ or the variation of field current (I_f), considering the sign of phase difference between voltage and current. In fact, this study improved the main criterion adopted in [8] and used it as a sub-criterion of this study. Accordingly, in the motoring mode, the negative and positive values of θ show the over excitation ($\Delta I_f/\Delta t > 0$) and under excitation actions ($\Delta I_f/\Delta t < 0$) of a motor, respectively. However, the generator operation is completely in the opposite way. This issue can be seen obviously in Figure 6. Consequently, Eq. (11) is considered as the first prerequisite of the proposed technique for RPD [27]:

$$\left(\frac{|E_A|}{|V_\phi|} > 1 \quad \text{and} \quad \frac{\Delta I_f}{\Delta t} > 0\right)(\measuredangle V - \measuredangle I) < 0,$$

$$\left(\frac{|E_A|}{|V_\phi|} < 1 \quad \text{and} \quad \frac{\Delta I_f}{\Delta t} < 0\right)(\measuredangle V - I\measuredangle) > 0. \quad (11)$$

In addition to the sign of the phase difference between V and I or (θ), the value of θ is of prime importance. This is because in the motoring mode, the stator current shifts at a value of 180°. In other words, in the motoring condition, θ should range from 90° to 270° (as mentioned in Section 2). To this end, the application of a directional block in the proposed angular-based relay is essential.

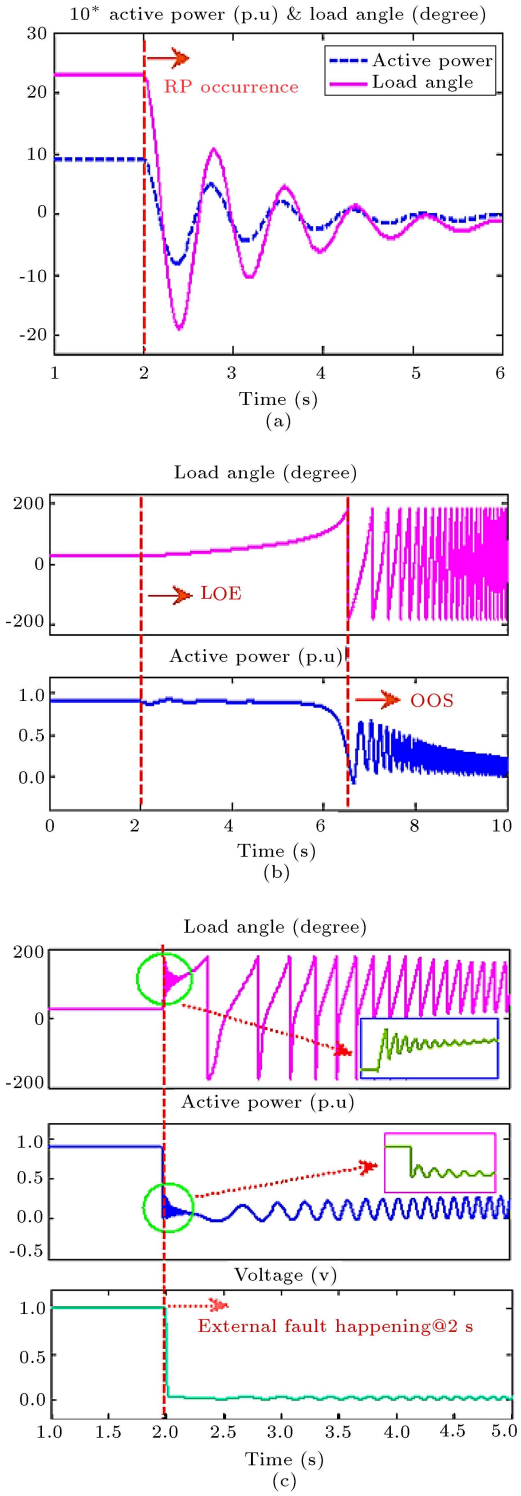

Figure 5. The behavior of a synchronous generator following: (a) RPC, (b) LOE, and (c) external fault.

However, the second prerequisite of the proposed algorithm is based on the value of voltage. According to Figure 5, LOE and OOS faults lead to impressive voltage drop in the generator terminal, while in RPC,

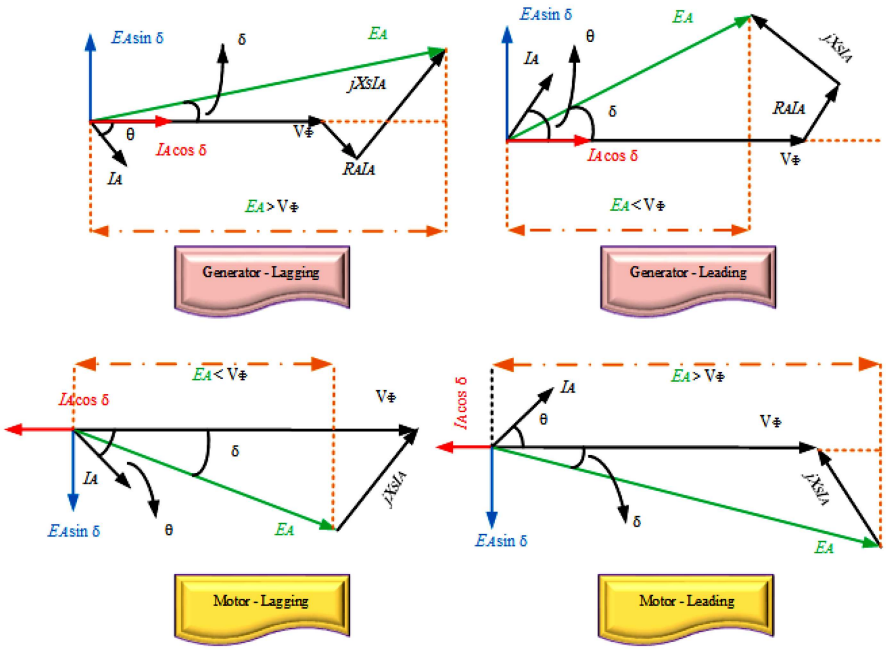

Figure 6. The phasor diagram of a synchronous machine in various operating conditions.

V shows minimum oscillation [7]. In other words, the value of V is always larger than 0.95 p.u, following RPC. As a result, this criterion can help the relay to discriminate RPF from external short-circuit faults, LOE, and unwanted power swings.

The third prerequisite for RPD refers to the variations of P and δ. As shown earlier in Figure 5, at initial moments of RPF inception, P and δ exhibit decreasing behavior. As a result, both ΔP and $\Delta\delta$ will be negative and their multiplication will be positive. Therefore, the following relation can be considered as the complementary prerequisite of the proposed algorithm.

$$\Delta P \times \Delta\delta > 0. \tag{12}$$

Finally, the key utilized criterion for RPD in this contribution is on the basis of the sign of vertical component of E_A ($E_A \sin\delta$) and, also, the sign of tangential component of I_A on V ($I_A \cos\theta$). In accordance to Figure 6, since δ is negative in a motoring condition, $E_A \sin\delta$ becomes negative in this mode. In other words, $E_A \sin\delta$ is expected to be negative, following RPF. However, in the generating mode, $E_A \sin\delta$ is positive since δ is positive in this condition. On the other hand, in the motoring condition, θ should be in the second or third quarter ($90 < \theta < 270$), as expressed in Section 2. Since $\cos\theta$ is negative in the mentioned range, $I_A \cos\theta$ is expected to be negative under RPC, while this value is positive in the generating mode. Accordingly, the final Proposed Reverse Power Detection Index (RPDI) of this study can be summarized as follows:

$$RPDI = E_A \sin\delta < 0 \quad \text{or} \quad I_A \cos\theta < 0. \tag{13}$$

4.2. Adjusting T_{RP}

As previously mentioned, both P and δ share identical behavior following RPF. Consequently, the derivatives of both P and δ oscillate in a unique range of frequencies. This frequency (f_{sw}) is in the range of 0.3 to 7 Hz [29]. Accordingly, the periods of $d\delta/dt$ and dP/dt are both between 0.142 and 3.33 s. As a result, the longest expected period for $d\delta/dt$ to become zero takes 1/4 of the period ($T_{sw}/4$), which is equal to 0.833 s. Therefore, RPF can be diagnosed after at most 0.833 s from the start of oscillations. By considering a secure margin of 8%, the final time interval (T_{RP}) can be obtained according to Eq. (14). This time interval is equal to 0.9 s and can be a suitable criterion for discriminating RPF with a sub-synchronous condition and Stable Power Swing (SPS).

$$T_{RP} = 1/08 \times (1/4) \times T_{sw}. \tag{14}$$

4.3. The flowchart of the proposed technique

Figure 7 depicts the algorithm of the proposed technique. As shown, the current and voltage phasors of the machine are measured. Consequently, the values of θ, V, and Eq. (11), as the initial prerequisites of RPD, are checked. Then, the values of P, E_A, and δ are obtained considering the measured quantities and mentioned relations, and the multiplication of both P and δ variations is evaluated as the complimentary prerequisite of the proposed method. Ultimately, the main index of the proposed scheme (RPDI) is analyzed at the predefined time. In order to ensure the algorithm security in the SPS condition, RPDI is searched by the algorithm for a preset time interval (T_{RP}), which is calculated via Eq. (14).

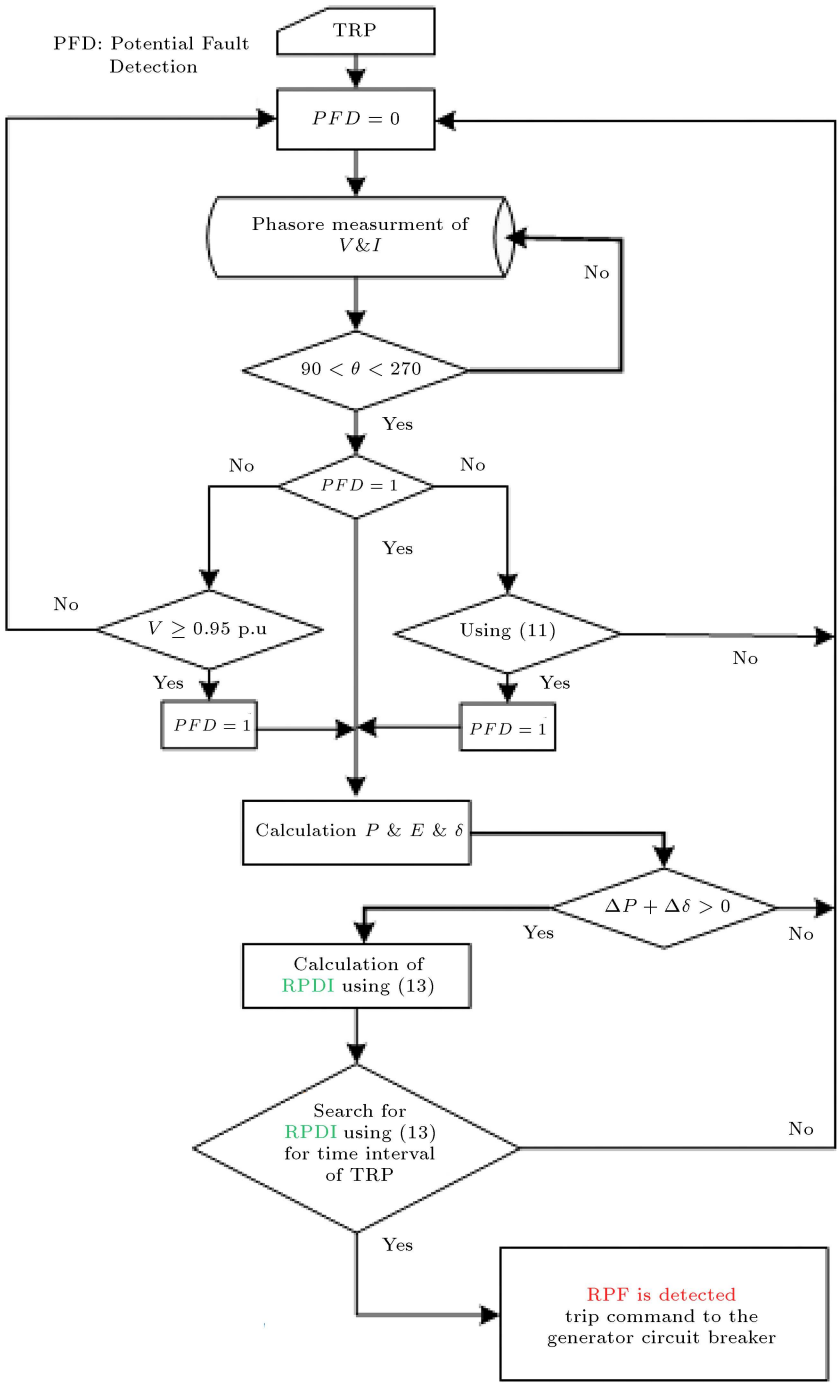

Figure 7. The flowchart of the proposed method.

In fact, this algorithm presents an improved technique with almost identical parameters, lower fault detection time, and better fault diagnosis than the parameter-based algorithm [8], which was previously investigated by the authors. The authors improved the main criterion of parameter-based method, utilized it as a sub-criterion, and also added the voltage condition for the most secure fault discrimination between RPC with LOE, OOS and SPS. The reverse power index (Eq. (13)) has been added to the algorithm as the main and final decision index for a fast and reliable RPF detection.

5. Evaluating the performance of the proposed angular-based RPD technique

The objective of this section is to evaluate the performance of the developed scheme. To this end, different extensive simulations are carried out considering various operating modes of a synchronous machine on

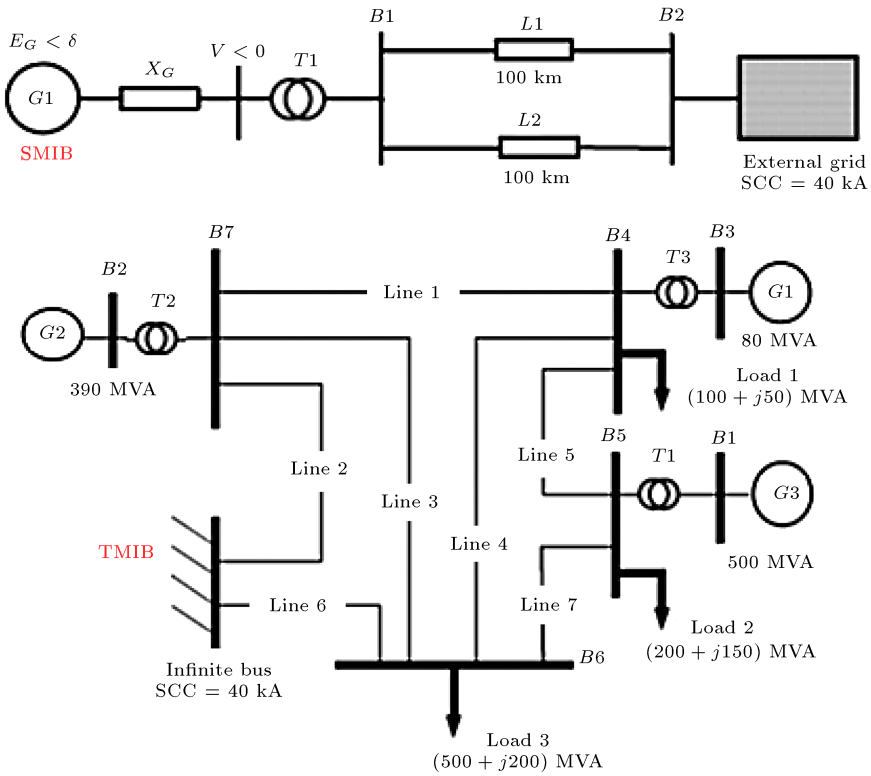

Figure 8. Configurations of SMIB and TMIB system.

two sample systems including a Single-Machine Infinite Bus (SMIB) system and a Three-Machine Infinite Bus (TMIB) system (see, Figure 8) [13]. In this study, a real bank test of the SMIB and TMIB power networks is utilized and the final simulation results, which are evaluated in Matlab software, are presented in Tables 2–5. It is notable that all the generators are equipped with Power System Stabilizer (PSS) and excitation system, and machine 2 of TMIB system is protected by the proposed angular-based RPR. Complementary details about the decisive quantities of the simulated systems are given in Appendices A and B (Tables A.1, A.2, B.1, and B.2) [7,13,21]. Besides, to present a better view of the simulation, a snap shot of one of the simulating conditions implemented in the MATLAB/ Simulink software considering RPC in SMIB system with hydraulic turbine as the prime mover and under inductive loading is shown in Appendix C (Figure C.1).

5.1. *Performance assessment on SMIB configuration*

This section carries out different extensive simulations in order to verify the correct operation of the proposed angular-based RPR on SMIB system in four subsections considering various potential conditions following an RPF below. It is noteworthy that the effect of the generator reactance has been considered in the loadings of the generator:

- **Heavy inductive loading (Mode 1)**; The prime mover: Steam turbine and hydraulic turbine; Droop settings of governor (1.01, 1.03, 1.05);
- **Light inductive loading (Mode 2)**; The prime mover: Steam turbine and hydraulic turbine; Droop settings of governor (1.01, 1.03, 1.05);
- **Heavy capacitive loading (Mode 3)**; The prime mover: Steam turbine and hydraulic turbine; Droop settings of governor (1.01, 1.03, 1.05);
- **Light capacitive loading (Mode 4)**; The prime mover: Steam turbine and hydraulic turbine; Droop settings of governor (1.01, 1.03, 1.05).

The final evaluation results of the proposed scheme in the SMIB network are given in Table 2. In order to show the variations of δ and θ in a unique figure and demonstrate complete oscillations of δ, the wave forms of δ are shown by multiplying its value by 5 or 10.

5.1.1. Heavy inductive loading (Mode 1)

Figure 9 shows the behavior of P, V, θ, δ, $I_A \cos\theta$, and $E_A \sin\delta$ of a synchronous machine under heavy inductive loading (Mode 1) utilizing two different turbines (hydraulic and steam) as the prime mover with droop setting of 1.01. This figure depicts the issued trip signals of the proposed technique. The generator loses its mover at $t = 2$ s. In the mentioned condition, the angular-based relay issues the trip signal at 0.085 s for steam turbine and 0.19 s for hydraulic turbine. It

Table 2. Angular-based relay operation in SMIB system.

	Initial loading (p.u)		Hydraulic turbine droop setting of governor			Steam turbine droop setting of governor		
			1.05	1.03	1.01	1.05	1.03	1.01
Mode	P	Q	Detection time (s)			Detection time (s)		
1	0.9	0.3	0.191	0.190	0.190	0.085	0.085	0.085
2	0.1	0.2	0.150	0.150	0.150	0.077	0.077	0.076
3	0.7	−0.5	0.194	0.193	0.193	0.086	0.086	0.086
4	0.3	−0.2	0.181	0.181	0.180	0.085	0.085	0.084

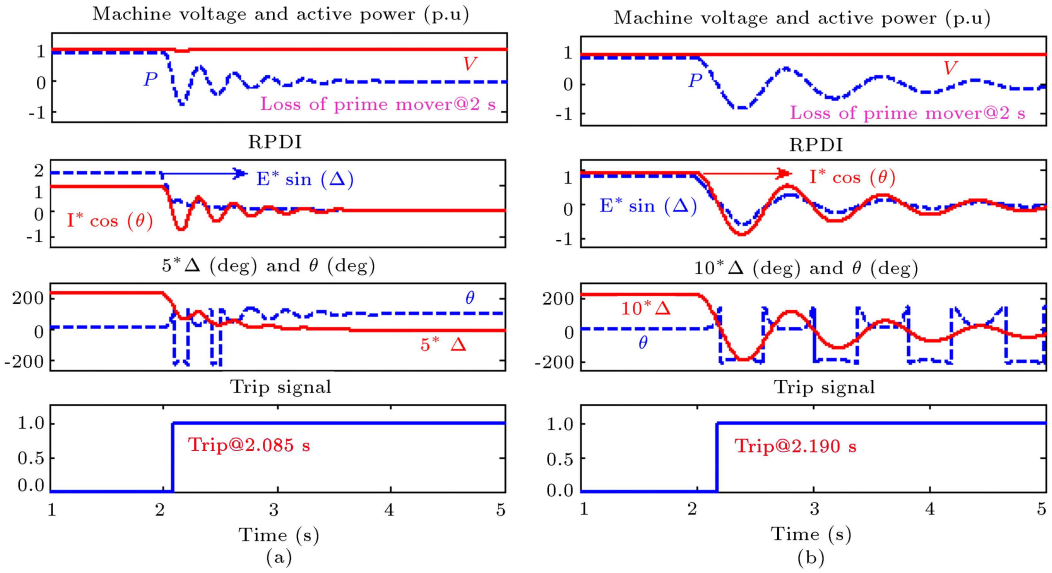

Figure 9. Variations in P, V, θ, δ, $I_A \cos\theta$, and $E_A \sin\delta$ of a synchronous machine and the trip signal of the proposed relay following RPF, with (a) steam turbine, considering Mode 1 and (b) hydraulic turbine, considering Mode 1.

is notable that the operation of the proposed relay for droop settings of 1.03 and 1.05 is also evaluated and the satisfying results are presented in Table 2.

5.1.2. Light inductive loading (Mode 2)

Figure 10 shows the behavior of the same generator parameters, as depicted in Figure 11, for light inductive loading using both hydraulic and steam turbines as the prime mover with a droop setting of 1.01. Accordingly, in Mode 2 of operation, the suggested relay trips at 0.076 s for steam turbine and 0.15 s for hydraulic turbine. Based on the evaluation results extracted from simulations of Modes 1 and 2, it can be obviously seen that the trip times of the proposed RPR are slightly different for the applied prime movers. The reason why this phenomenon exists stems from the structural differences between steam and hydraulic turbines and governors.

5.1.3. Heavy capacitive loading (Mode 3)

In order to complete the assessment of the suggested scheme, the effects of capacitive loadings on the angular-based relay are evaluated for both steam and hydraulic turbines. Accordingly, Figure 11 shows the behavior of P, V, θ, δ, $I_A \cos\theta$, and $E_A \sin\delta$ of a synchronous generator for both steam and hydraulic turbines under heavy capacitive loading (Mode 3). In this condition, the angular-based relay sends the trip command at 0.086 s for steam turbine and 0.193 s for hydraulic turbine. It should be noticed that the operation of the angular-based relay for two other droop settings of governor is also evaluated and the satisfying results are shown in Table 2.

5.1.4. Light capacitive loading (Mode 4)

Figure 12 shows the behavior of the same parameters of the studied synchronous generator, as depicted in Figure 11, for light capacitive loading using both hydraulic and steam turbines as the prime mover with droop setting of 1.01. Accordingly, in Mode 4, the relay trips at 0.084 s and 0.180 s for steam and hydraulic

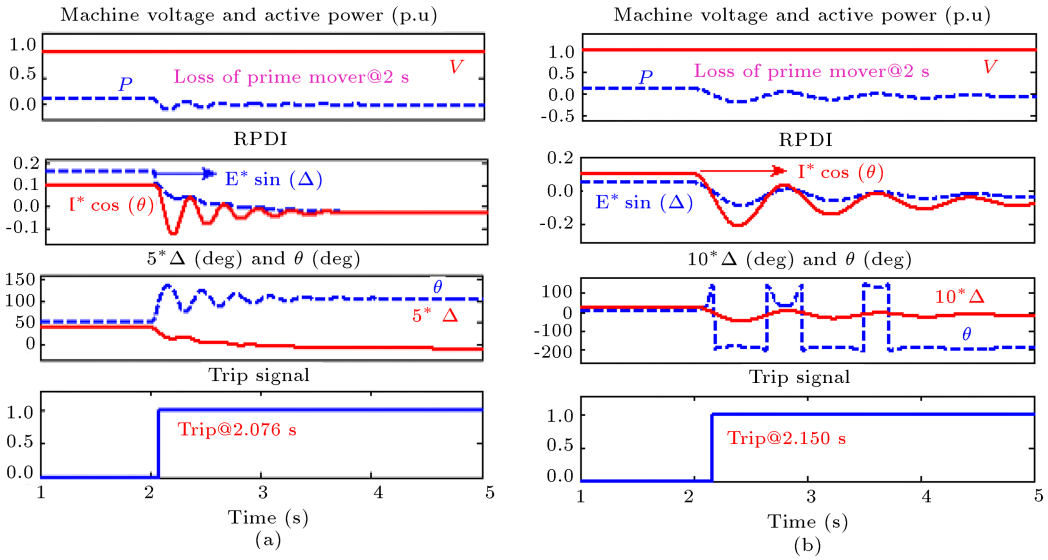

Figure 10. Variations in in P, V, θ, δ, $I_A \cos\theta$, and $E_A \sin\delta$ of a synchronous machine and the trip signal of the proposed relay following RPF, (a) steam turbine, considering Mode 2 and (b) hydraulic turbine, considering Mode 2.

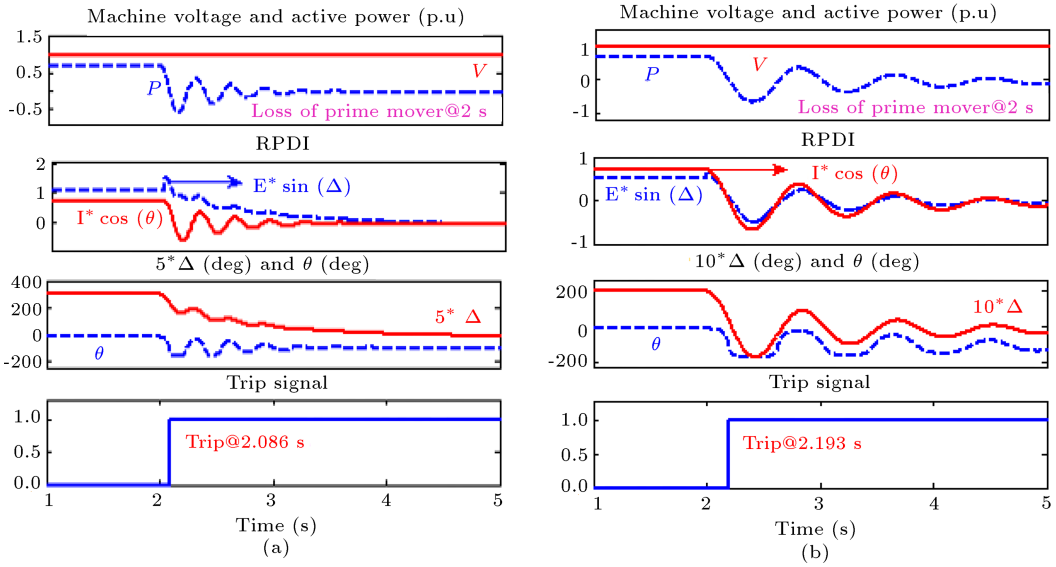

Figure 11. Variations in in P, V, θ, δ, $I_A \cos\theta$, and $E_A \sin\delta$of a synchronous machine and the trip signal of the proposed relay following RPF, with (a) steam turbine, considering Mode 3 and (b) hydraulic turbine, considering Mode 3.

turbines, respectively. Of note, in all the simulated modes, the RPC occurs at $t = 2$ s. According to the relay performance in Modes 3 and 4, it can be concluded that due to structural differences between steam and hydraulic turbines, the trip times slightly differ for two prime movers in the mentioned modes, which is not significant and is almost ignorable (exactly the same as Modes 1 and 2).

5.1.5. Final results

The final simulation results of the studied generator under 4 different loadings and 3 different droop settings of governor for both steam and hydraulic turbines are summarized in Table 2. Accordingly, the load changes have slight effect on the operation of the angular-based RPR. V_ϕ, E_A and the magnetic flux of the machine are controlled by the Automatic Voltage Regulator (AVR) in different loadings. Furthermore, the simulation results demonstrate that the action time of the angular-based relay is almost identical for all droop settings of the prime mover, because the governor droop setting is known as a mechanical quantity, whereas the angular-based RPR performs on the basis of electrical quantities.

5.2. Performance assessment on TMIB configuration

To conduct a deep analysis on the satisfactory per-

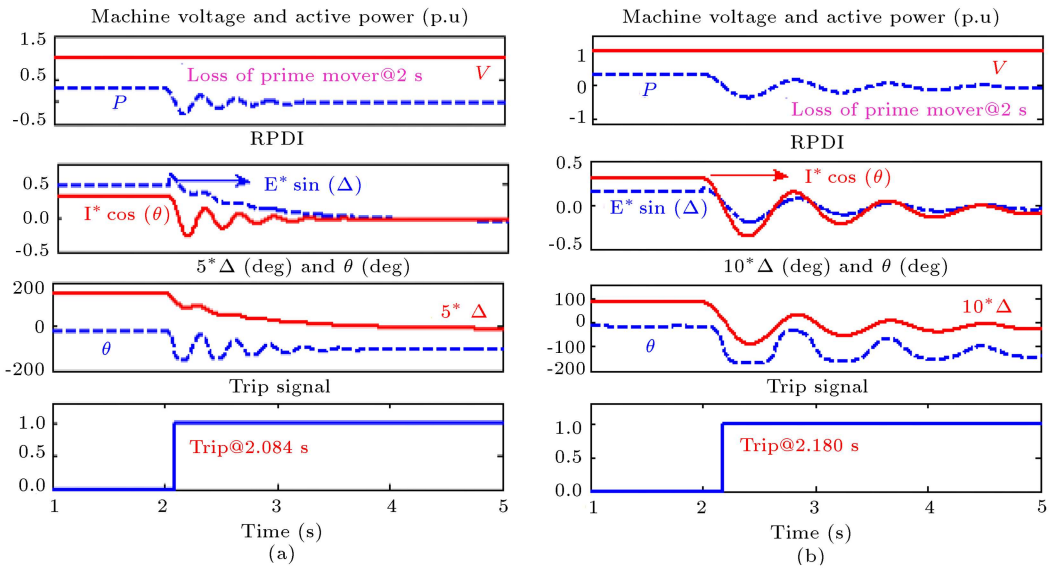

Figure 12. Variations in P, V, θ, δ, $I_A \cos\theta$, and $E_A \sin\delta$ of a synchronous machine and the trip signal of the proposed relay following RPF, with (a) steam turbine, considering Mode 4 and (b) hydraulic turbine, considering Mode 4.

Table 3. Angular-based relay operation in TMIB system.

	Initial loading (p.u)		Hydraulic turbine droop setting of governor			Steam turbine droop setting of governor		
			1.05	1.03	1.01	1.05	1.03	1.01
Mode	P	Q	Detection time (s)			Detection time (s)		
1	0.9	0.3	0.242	0.242	0.241	0.124	0.124	0.122
2	0.1	0.2	0.214	0.216	0.212	0.118	0.118	0.118
3	0.7	−0.5	0.249	0.248	0.245	0.125	0.124	0.124
4	0.3	−0.2	0.242	0.241	0.230	0.120	0.120	0.120

formance of the suggested method, the stability and accuracy of the proposed angular-based RPR are also verified in a TMIB network as the final validation. In this system, generator 2 is protected by the proposed angular-based relay. The performance of the proposed relay has been simulated for both steam and hydraulic turbines, considering 3 different droop settings of the prime mover governor and various loading points including heavy and light inductive loading (Modes 1 and 2) and, also, heavy and light capacitive loading (Modes 3 and 4). The final simulation results are summarized in Table 3. Accordingly, the introduced RPD technique had a fast, secure and reliable performance in all the scenarios. Comparative evaluation of the proposed method in the case of SMIB and TMIB configurations shows a very small extension in trip time of the RPR in the TMIB system. Nevertheless, this time expansion is quite negligible and does not affect the satisfying performance of the angular-based relay.

In order to complete the analysis of the angular-based relay performance in the TMIB network, all the possible modes of the generator loading with a hydraulic turbine as the prime mover were studied. Accordingly, Figure 13 shows the changes in P, V, θ, δ, $I_A \cos\theta$, and $E_A \sin\delta$ of a synchronous generator and the issued trip signal of the suggested relay for the hydraulic turbine under heavy inductive loading (Mode 1) and light inductive loading (Mode 2). In Mode 1, the angular-based relay trips at 0.241 s, whereas in Mode 2, the corresponding time is 0.212 s.

Figure 14 shows the variations of P, V, θ, δ, $I_A \cos\theta$, and $E_A \sin\delta$ and the trip signal of the proposed relay for the hydraulic turbine under heavy capacitive loading (Mode 3) and light capacitive loading (Mode 4). Accordingly, the trip signals have been sent by the angular-based relay at 0.245 s and 0.230 s for Modes 3 and 4, respectively.

It is noteworthy that the behavior of the proposed protection technique has been evaluated for steam turbine under heavy inductive loading (Mode 1). Fig-

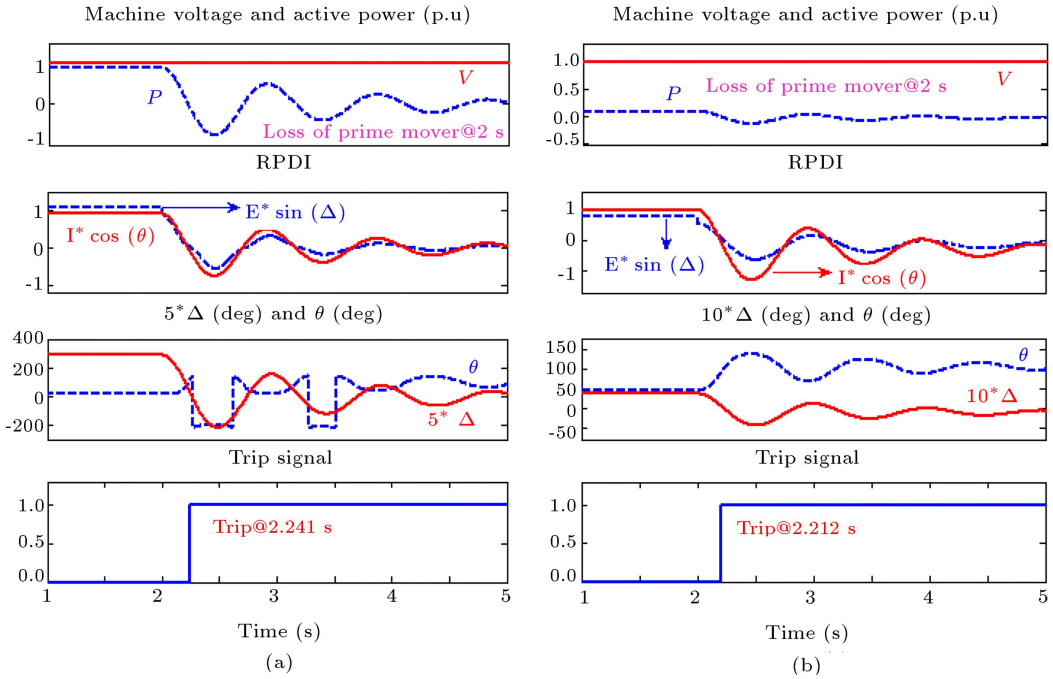

Figure 13. Variations in P, V, θ, δ, $I_A \cos\theta$, and $E_A \sin\delta$ of a synchronous machine in a TMIB system and the trip signal of the proposed relay following RPF, with (a) hydraulic turbine, considering Mode 1 (b) hydraulic turbine, considering Mode 2.

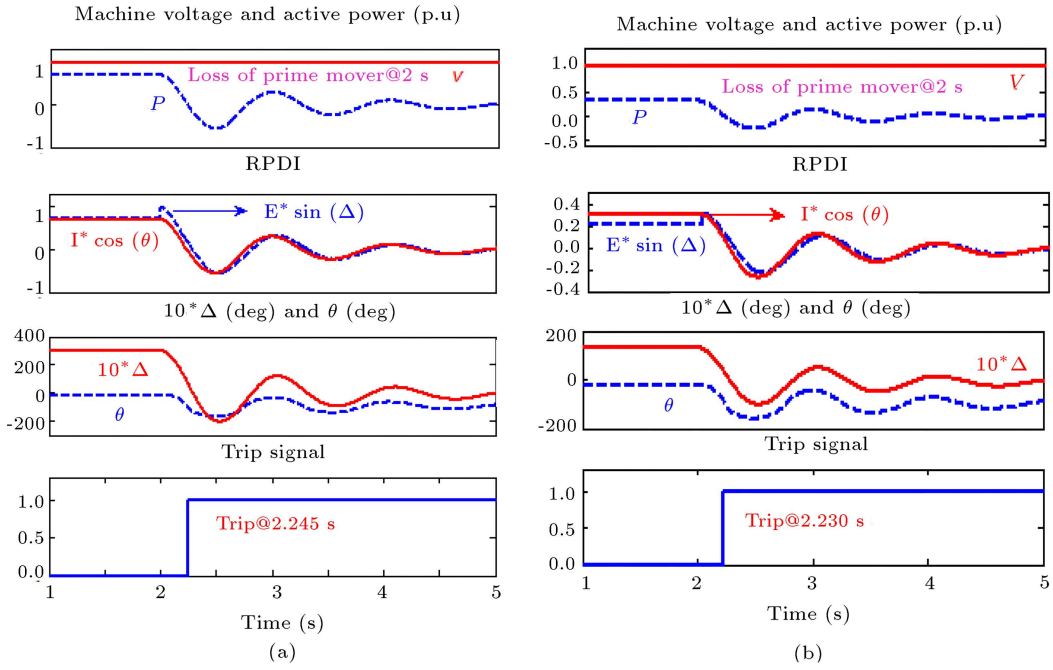

Figure 14. Variations in P, V, θ, δ, $I_A \cos\theta$, and $E_A \sin\delta$ of a synchronous machine in a TMIB system and the trip signal of the proposed relay following RPF, with (a) hydraulic turbine, considering Mode 3 and (b) hydraulic turbine, considering Mode 4.

ure 15 shows the behavior of the same parameters of the studied synchronous generator, as depicted in Figures 13 and 14. Accordingly, the proposed RP relay sends the trip signal at 0.122 s under heavy inductive loading, while the generator is rotated by a steam turbine, which shows the fast performance of the relay.

6. Comparative analysis

6.1. Comparison of different methods

This section aims to compare the performance of the angular-based relay with those of other existing schemes including directional3, flux-based [7], and

Table 4. Performance comparison of RPC detection schemes.

Method of protection	Hydraulic turbine droop= 1.01 p.u Loading type (p.u)		Steam turbine droop= 1.01 p.u Loading type (p.u)	
	Mode 1	Mode 4	Mode 1	Mode 4
	Detection time (s)		Detection time (s)	
Directional	7.98	7.96	7.2	7.16
Flux-based	0.50	0.516	0.17	0.17
Parameter-based	0.385	0.394	0.15	0.15
Angular-based	0.190	0.180	0.085	0.084

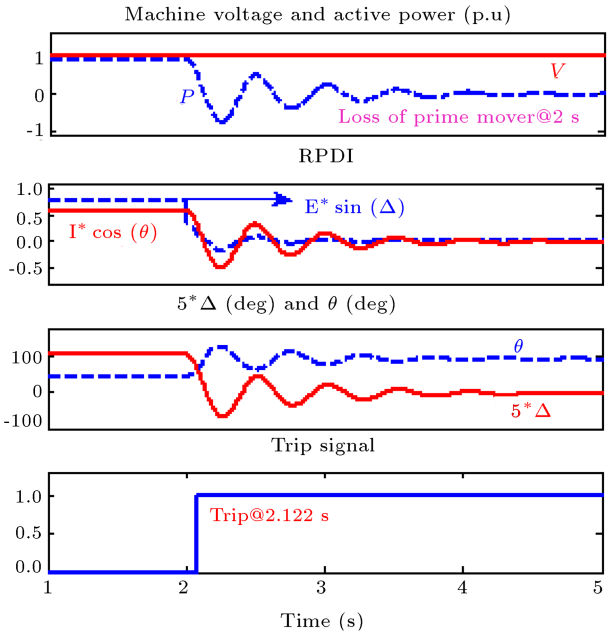

Figure 15. Variations in P, V, θ, δ, $I_A \cos\theta$, and $E_A \sin\delta$ of a synchronous machine in a TMIB system and the trip signal of the proposed relay following RPF, with a steam turbine, considering Mode 1.

parameter-based technique [8]. To this end, the trip times of the relays in RPC are compared together for both steam and hydraulic turbines, considering Modes 1 and 4 of loading and the results are summarized in Table 4. Accordingly, the performance of the parameter-based method is faster and more reliable than both flux-based and directional techniques. For instance, in Mode 1, the parameter-based, flux-based, and the directional relay issue the trip signal at 0.385 s, 0.5 s, and 7.98 s, respectively, after the RPF inception for hydraulic turbine. However, the corresponding values are 0.15 s, 0.17 s, and 7.2 s for steam turbines.

However, the simulations of the suggested method in the sample networks demonstrate that the angular-based relay has the fastest and the most secure performance among all the introduced methods. In Mode 1, the angular-based relay sends the trip signal at 0.19 s for hydraulic and 0.085 s for the steam turbine. However, the corresponding trip time values are 0.18 s and 0.084 s for Mode 4. Thus, utilization of angular-based RPR can decrease the generator motoring time effectively, which leads to decrement in mechanical stress and the risk of damage to the mover.

6.2. Comparison of the proposed method for different sizes of generators

Eventually, the operation of the angular-based RPR has been evaluated for various sizes of generators with two movers, i.e., steam and hydraulic turbines, considering Modes 1 and 4 of loading, and the final results are presented in Table 5. Accordingly, the generator size has no significant effect on the performance of the proposed scheme in all the scenarios.

7. Conclusion

This contribution proposed a fast predictive technique to diagnose Reverse Power Condition (RPC) based on variations of angular parameters in synchronous generators. In fact, the authors introduced an improved method in comparison with the parameter-based method, with almost the same applied parameters, but with higher operation speed and better fault discrimination. Extensive simulations were conducted on two sample networks (Single-Machine Infinite Bus (SMIB) and Three-Machine Infinite Bus (TMIB)), which represented the angular-based relay independence from the generator size, loading, and droop setting of governor. The obtained results also demonstrated the fastest and the most secure performance of the angular-based relay compared to directional, flux-based, and parameter-based techniques. Accordingly, for hydraulic turbines, the proposed method sent the trip signal at 0.19 s and 0.18 s after Reverse Power (RP) inception for Modes 1 and 4, respectively. The corresponding values were 0.085 s and 0.084 s for steam turbines. Therefore, the fast performance of the angular-based RP method led to effective decrement of the mechanical stress on the

Table 5. Performance comparison of the suggested technique, considering different sizes of generators.

	Hydraulic turbine droop= 1.01 p.u Loading type (p.u)		**Steam turbine droop= 1.01 p.u Loading type (p.u)**	
Generator power (MVA)	**Mode 1**	**Mode 4**	**Mode 1**	**Mode 4**
	Detection time (s)		**Detection time (s)**	
390	0.190	0.180	0.075	0.075
555	0.223	0.211	0.084	0.083
600	0.229	0.218	0.085	0.084

turbo compressor shaft as well as the potential risks to the prime mover.

List of symbols

V_ϕ	Generator terminal voltage
I_A	Generator terminal current
E_A	Generator internal voltage
R_A	The stator winding resistance of the generator
X_S	Generator synchronous reactance
δ	Load angle
θ	Phase difference between voltage and current
B_r	Rotor magnetic field
B_s	Stator magnetic field
Z	Impedance
φ	Air-gap magnetic flux
	Active power
P_M	Mechanical input power
H	Inertia constant
f_0	Fundamental frequency
ω	Measured speed of the generator
ω_0	Synchronous speed of the generator
f_{slip}	Active power oscillation frequency
I_f	Field current
$\measuredangle V$	The phase of voltage
$\measuredangle I$	The phase of current
f_{sw}	Swing frequency
T_{sw}	Swing period
T_{RP}	Maximum time interval of the relay

List of abbreviations

RP	Reverse Power
RPC	Reverse Power Condition
RPD	Reverse Power Detection
RPR	Reverse Power Relay
RPP	Reverse Power Protection
RPF	Reverse Power Fault
LOE	Loss Of Excitation
OOS	Out Of Step
MTA	Maximum Torque Angle
SPS	Stable Power Swing
RPDI	Reverse Power Detection Index
PFD	Potential Fault Detection
SMIB	Single-Machine Infinite Bus
TMIB	Three-Machine Infinite Bus
PSS	Power System Stabilizer
AVR	Automatic Voltage Regulator

References

1. IEEE Guide for AC Generator Protection, IEEE Standard C37.102-2006, (Nov. 2006).

2. Clark, H.K. and Feltes, J.W. "Industrial and cogeneration protection problems requiring simulation", *IEEE Trans. Ind. Appl.*, **25**(4), pp. 766–775 (1989).

3. Aman, M., Jasmon, G., Khan, Q., et al. "Modeling and simulation of reverse power relay for generator protection", In: *IEEE International Power Engineering and Optimization Conference (PEDCO)*, Melaka, Malaysia, pp. 317–322 (June 2012).

4. Buque, C. and Chowdhury, S. "Modelling and simulation of reverse power relay for loss of mains protection of distributed generation in micro grids", In *IEEE Power and Energy Society General Meeting*, Vancouver, BC, Canada, pp. 1–5 (21-25 July 2013).

5. Jenkins, A., Duncan, J., and Lynch, CA. "Impact of steam turbine valve closure on a synchronous machine and its reverse power protection", *Proc. of 12th IET*

International Conference on Developments in Power System Protection (DPSP), Copenhagen, Denmark, pp. 1–6 (31 March-3 April 2014).

6. Nichols, W.H., and Castro, C.A. "Power System Phase Rotation and Polarized Protective Relays", *IEEE Transactions on Industry Applications*, **26**(6), pp. 1075–1080 (1990).
7. Yaghobi, H. "Fast predictive technique for reverse power detection in synchronous generator", *IET Electric Power Applications.*, **12**(4), pp. 508–517 (2018).
8. Samami, M. and Niaz Azari, M. "Novel fast and secure approach for reverse power protection in synchronous generators", *IET Electric Power Applications*, **13**(12), pp. 2128–2138 (2019).
9. Ostojić, M. and Djurić, M. "The algorithm for the detection of loss of excitation of synchronous generators based on a digital-phase comparator", *Electrical Engineering*, **100**(2), pp. 1287–1296 (2018).
10. Yaghobi, H. "A new adaptive impedance-based LOE protection of synchronous generator in the presence of STATCOM", *IEEE Trans. Power Del.*, **32**(6), pp. 2489–2499 (2017).
11. Mahamedi, B., Zhu, J.G., and Hashemi, S.M. "A setting-free approach to detecting loss of excitation in synchronous generators", *IEEE Trans. Power Del.*, **31**(5), pp. 2270–2278 (2016).
12. Hasani, A. and Haghjoo, F. "Fast and secure detection technique for loss of field occurrence in synchronous generators", *IET Electric Power Applications*, **11**(4), pp. 567–577 (2017).
13. Hasani, A. and Haghjoo, F. "A secure and setting-free technique to detect loss of field in synchronous generators", *IEEE Trans. Energy Conv.*, **32**(4), pp. 1512–1522 (2017).
14. Amini, M., Davarpanah, M., and Sanaye-Pasand, M. "A novel approach to detect the synchronous generator loss of excitation", *IEEE Trans. Power Del.*, **30**(3), pp. 1429–1438 (2015).
15. Yaghobi, H. "Fast discrimination of stable power swing with synchronous generator loss of excitation", *IET Gen. Transm. Distrib*, **10**(7), pp. 1682–1690 (2016).
16. Niaz Azari, M. "A setting-free flux-based synchronous generator loss of excitation protection", *Electrical Engineering.*, **100**(4), pp. 2329–2339 (2018).
17. Abedini, M., Sanaye-Pasand, M., and Davarpanah, M. "Loss-of-field detection relay based on rotor signals estimation", *IEEE Trans. Power Deliv.*, **33**(2), pp. 779–788 (2018).
18. Noroozi, N., Yaghobi, H., Alinejad-Beromi, Y. "Analytical technique for synchronous generator loss-of-excitation protection", *IET Generation, Transmission and Distribution*, **11**(9), pp. 2222–2231 (2017).
19. Abedini, M., Davarpanah, M., Sanaye-Pasand, M., et al. "Generator out-of- step prediction based on faster-than-real-time analysis: Concepts and Applications", *IEEE Trans. on Power Systems*, **33**(4), pp. 4563–4573 (2018).
20. Zhang, S. and Zhang, Y. "A novel out-of-step splitting protection based on the wide area information", *IEEE Transactions on Smart Grid*, **8**(1), pp. 41–51 (2017).
21. Paudyal, S., Ramakrishna, G., and Sachdev, M. "Application of equal area criterion conditions in the time domain for out-of-step protection", *IEEE Trans. Power Del.*, **25**(2), pp. 600–609 (2010).
22. Ariff, M. and Pal, B. "Adaptive protection and control in the power system for wide-area blackout prevention", *IEEE Trans. Power Del.*, **31**(4), pp. 1815–1825 (2016).
23. Alinezhad, B. and Karegar, H.K. "Out-of-step protection based on equal area criterion", *IEEE Trans. Power Syst.*, **32**(2), pp. 968–977 (2017).
24. Alinezhad, B. and Karegar, H.K. "Predictive out of step relay based on equal area criterion and PMU data", *International Transactions on Electrical Energy Systems*, **27**(7), e2327 (2017).
25. Phadke, A. and Thorp, J., *Computer Relaying for Power Systems*, New York: John Wiley and Sons (2009).
26. Holguin, J.P., Rodriguez, D.C., and Ramos, G. "Reverse power flow (RPF) detection and impact on protection coordination of distribution systems", *IEEE Trans. on Indust. App.*, **56**(3), pp. 2393–2401 (2020).
27. Chapman, S., *Electric Machinery Fundamentals*, New York: Tata McGraw-Hill Education, Fourth Ed. (2005).
28. Mazhari, S.M., Khorramdel, B.C., Chung, Y., et al. "A simulation-based classification approach for online prediction of generator dynamic behavior under multiple large disturbances", *IEEE Trans. on Power Systems*, **36**(2), pp. 1217–1228 (2021).
29. Mahamedi, B. and Zhu, J.G. "A novel approach to detect symmetrical faults occurring during power swings by using frequency components of instantaneous three-phase active power", *IEEE Trans. Power Del.*, **27**(3), pp. 1368–1376 (2012).

Appendix A

This appendix includes two tables. Table A.1 represents data for SMIB network and Table A.2 represents data for TMIB network.

Appendix B

This appendix includes two tables. Table B.1 represents data of the utilized hydraulic and steam turbines and Table B.2 represents data of the utilized AVR and PSS.

Table A.1. Data of SMIB network [7,13].

With steam turbine	**With hydraulic turbine**
$S = 600$ MVA, $f = 60$ Hz, $V = 22$ kv	$S = 390$ MVA, $f = 60$ Hz, $V = 24$ kv
$X_d = 1.65$ p.u, X'_d (p.u) $= 0.25$ p.u	$X_d = 1.35$ p.u, X'_d (p.u) $= 0.296$ p.u
$X''_d = 0.2$ p.u, $X_q = 1.59$ p.u	$X''_d = 0.252$ p.u, $X_q = 0.474$ p.u
$X'_q = 0.46$ p.u, $X''_q = 0.2$ p.u	$X''_q = 0.243$ p.u, $X_1 = 0.18$ p.u
$X_1 = 0.14$ p.u, $T'_{do} = 4.5$ s	$T'_{do} = 5$ s, $T''_{d0} = 0.1$ s
$T''_{d0} = 0.04$ s, $T'_{qo} = 0.67$ s	$T''_{qo} = 0.09$ s, $R_s = 0.0028$ p.u
$T''_{qo} = 0.09$ s, $R_s = 0.0045$ p.u	
Inertia constant (H) $= 0.8788$ s	Inertia constant (H) $= 5.5$ s
Transformer = j0.15 p.u , Transmission line = j0.5 p.u	

Table A.2. Data of TMIB network [7,8].

Generators
G1: $S = 80$ MVA, $V = 13.8$ kv, $H = 3.5$ s
G2: $S = 390$ MVA, $V = 13.8$ kv, $H = 5.5$ s
G3: $S = 500$ MVA, $V = 13.8$ kv, $H = 4.0$ s
Transmission lines
L1: $Z = 0.048 + \text{j}0.48\ \Omega$, **L2**: $Z = 0.00576 + \text{j}0.573\ \Omega$
L3: $Z = 0.0288 + 0.288\ \Omega$, **L4**: $Z = 0.0576 + \text{j}0.576\ \Omega$
L5: $Z = 0.0142 + \text{j}0.142\ \Omega$, **L6**: $Z = 0.00192 + \text{j}0.192\ \Omega$
L7: $Z = \text{j}0.0957\ \Omega$

Table B.1. Data of the utilized hydraulic and steam turbines [7,8,18].

Steam turbine													
T_{sr}	T_{sm}	k_p	F_2	F_3	F_4	F_5	T_2	T_3	T_4	T_5	$g_{\min}$	$V_{g\min}$	$g_{\max}$	$V_{g\max}$
0.001 s	0.15 s	1	0.5	0.5	0	0	0 s	10 s	3.3 s	0.5 s	0 p.u	−0.1 p.u/s	4.496 p.u	0.1 p.u/s
Hydraulic turbine													
k_a	T_a	k_p		k_i		k_d	T_d	β	T_w	$g_{\min}$	$V_{g\min}$	$g_{\max}$	$V_{g\max}$	
3.33 p.u	0.07 s	1.163		0.105		0	0.01 s	0	2.67 s	0.01 p.u	−0.1 p.u/s	0.975 p.u	0.1 p.u/s	

Table B.2. Data of the utilized AVR and PSS [7,8,18].

Alternative Voltage Regulator (AVR)								
T_r	k_a	T_a	k_f	T_f	k_e	T_e	$V_{f\max}$	$V_{f\min}$
0.02 s	300 p.u	0.001	0.001 p.u	0.1 s	1 p.u	0 s	11.5 p.u	−11.5 p.u
Power System Stabilizer (PSS)								
k_p	T_w	T_{1n}	T_{1d}	T_{2n}	T_{2d}	$V_{s\max}$	$V_{s\min}$	
30 p.u	10 s	0.05 s	0.02 s	3 s	5.4 s	0.15 p.u	−0.15 p.u	

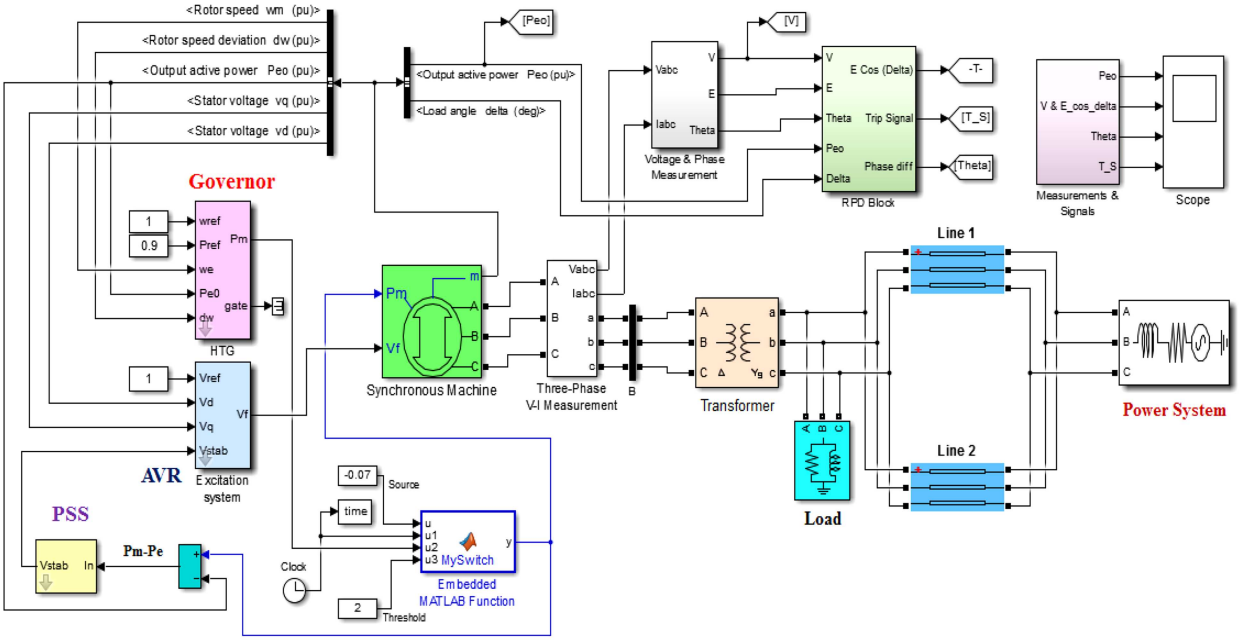

Figure C.1. A view of SMIB simulated model in MATLAB/Simulink.

Appendix C

This appendix includes one figure. Figure C.1 shows a view of SMIB simulated model in MATLAB/Simulink.

Biographies

Mehdi Samami received his BSc degree in Electrical Engineering from South Tehran Branch, Islamic Azad University, Tehran, Iran in 2007 and obtained his MSc (2015) degree in the same field from Mazandaran Science and Research Branch, Islamic Azad University, Sari, Iran. He also received his PhD in Electrical Engineering from Sari Branch, Islamic Azad University, Sari, Iran in 2021. His research interests include analysis, design, and protection of electrical machines.

Milad Niaz Azari received his BSc degree in Electrical Engineering from Noshirvani University of Technology, Babol, Iran in 2007 and obtained his MSc (2009) and PhD (2013) in Electrical Engineering from Amir Kabir University of Technology, Tehran. Since 2014, he has been with University of Science and Technology of Mazandaran, Behshahr, Iran as an Assistant Professor. His areas of interest are electrical machines design and power electronics.